King Saud University

Arabian Journal of Chemistry

www.ksu.edu.sa
www.sciencedirect.com

ORIGINAL ARTICLE

Functionalization of sodium magnesium silicate hydroxide/sodium magnesium silicate hydrate nanostructures by chitosan as a novel nanocomposite for efficient removal of methylene blue and crystal violet dyes from aqueous media

Wejdan S. Albishri, Hanadi A. Katouah *

Department of Chemistry, Faculty of Applied Sciences, Umm Al-Qura University, Makkah 21955, Saudi Arabia

Abstract Herein, sodium magnesium silicate hydroxide/sodium magnesium silicate hydrate nanostructures were facilely synthesized using the hydrothermal method. After that, the synthesized nanostructures were modified by chitosan as a novel nanocomposite for the efficient removal of the methylene blue and crystal violet dyes from aqueous media. The synthesized nanostructures and their chitosan composite were characterized using several tools such as XRD, FT-IR, EDX, CHN, and SEM. The functionalization of nanostructures with chitosan led to the appearance of chitosan XRD peaks at $2\Theta = 8.9°$ and $21°$ whereas the intensities of the other XRD peaks were affected. The SEM analysis showed that the nanostructures consist of spheres and irregular shapes. Also, the nanocomposite consists of cotton and large irregular shapes due to the functionalization of the synthesized nanostructures with chitosan. Also, the EDX analysis confirmed that the nanocomposite consists of Si, Mg, Na, O, C, and N with weight percentages equal to 7.24%, 5.73%, 10.59%, 30.99%, 43.25%, and 2.20%, respectively. The CHN elemental analysis confirmed that the nanocomposite contained C, H, and N with weight percentages equal to 53.28%, 4.32%, and 1.92%, respectively. Hence, pH = 8, time = 50 min, and temperature = 298 K are the ideal values that achieves the maximum removal of the examined dyes. The maximum adsorption capacity of the nanostructures and nanocomposite toward the methylene blue dye is 19.07 and 20.25 mg/g, respectively. Also, the maximum adsorption capacity of the nanostructures and nanocomposite

* Corresponding author.
E-mail addresses: hanadikatouah@yahoo.com, hakatouah@uqu.edu.sa (H.A. Katouah).

Production and hosting by Elsevier

toward the crystal violet dye is 18.62 and 23.51 mg/g, respectively. The adsorption processes are chemical and exothermic. Besides, the adsorption processes followed the pseudo-second-order kinetic model and the Langmuir isotherm.

1. Introduction

According to the literature, 10–15% of the organic dyes used in human activities (often in the textile industry) can be released into the environment (Elgarahy et al., 2021; Oladoye et al., 2022). Due to the improper managing with these organic dyes and their discharge into the environment, there are severe pollution risks primarily associated with the retrogression of water quality, and hence endangering the health of the exposed population (Qiu et al., 2017; Sankar Sana et al., 2022). Based on their chemical structures, dyes can generally be divided into three categories: nonionic, cationic, and anionic (Konicki et al., 2015). Organic cationic dyes, such as crystal violet (CV) and methylene blue (MB), are considered to be more harmful than anionic ones (Adel et al., 2021; Fetimi et al., 2021; Karaman et al., 2022; Karimi-Maleh et al., 2023). The removal of MB and CV dyes then becomes a major area of study. Various techniques, including coagulation/flocculation, oxidation/ozone, membrane separation, photodegradation, adsorption, and biological processes, can be utilized to eliminate these toxic dyes and provide environmental protection (Abdelrahman et al., 2019b; Arif Ullah et al., 2023; El-Aassar et al., 2022; Hotan Alsohaimi et al., 2023; Mahmoud et al., 2019; Wang et al., 2022; Wasim et al., 2022). Diverse studies have concluded that most of these elimination techniques are insufficient for achieving a simple and effective treatment of dye-polluted water. In another sense, they may also be costly. To obtain treated water with the appropriate quality for human consumption and to protect the environment, it is necessary to employ an efficient and dependable removal technique. Due to its numerous benefits, including high removal efficiency and relatively low operating costs, the adsorption technique has been deemed a competitive removal method (Abdelrahman, 2018; Abdelrahman et al., 2019a). There are a lot of adsorbents for removing methylene blue and crystal violet dyes such as vilvam fruit shell carbon, zirconium silicate/SDS nanocomposite, carboxymethyl cellulose/ZSM-5/ZIF-8, magnetic cellulose beads, alginate grafted polyacrylonitrile beads, carboxymethyl cellulose/k-carrageenan/activated montmorillonite, alginate-grafted-poly (methyl methacrylate), and magnetic NaY zeolite (Liu et al., 2018; Luo and Zhang, 2009; Mahmoud et al., 2019; Marsiezade and Javanbakht, 2020; Priya et al., 2014; Salisu et al., 2015b, 2015a; Shirani et al., 2014). However, the majority of these adsorbents are prepared from expensive chemicals. Finding novel low-cost adsorbents with a high affinity for dye molecules is a necessary and urgent objective. So, in this work, sodium magnesium silicate hydroxide/ sodium magnesium silicate hydrate nanostructures were facilely synthesized then modified by chitosan as a novel nanocomposite. The synthesized nanocomposite was utilized for the efficient removal of methylene blue and crystal violet dyes from aqueous media. Effects of pH, time, temperature, and concentrations were studied. The novelty of the work is due to the following reasons;

1: In the crystal lattice of the sodium magnesium silicate hydroxide/sodium magnesium silicate hydrate nanostructures, some $Si(IV)$ ions is replaced by some $Mg(II)$ ions and hence a negative charge is produced and neutralized by sodium ions. After that, the sodium ions can easily be replaced by cationic molecules such as methylene blue and crystal violet dyes.

2: The functionalization of the synthesized nanostructures with chitosan makes the nanocomposite can remove the cationic dyes (i.e., methylene blue and crystal violet dyes) via chemical electrostatic attraction between dyes and functional groups (i.e., NH_2 and OH) of the nanocomposite in basic medium.

2. Experimental

2.1. Chemicals

Crystal violet dye ($C_{25}H_{30}ClN_3$), methylene blue dye ($C_{16}H_{18}N_3SCl$), hydrochloric acid (HCl), sodium metasilicate pentahydrate ($Na_2SiO_3 \cdot 5H_2O$), sodium hydroxide (NaOH), and magnesium chloride hexahydrate ($MgCl_2 \cdot 6H_2O$) were gotten from Sigma Aldrich Company and utilized without additional chemical refining. Also, chitosan was supplied via ROTH company, Germany.

2.2. Synthesis

2.2.1. Synthesis of sodium magnesium silicate hydroxide/ sodium magnesium silicate hydrate nanostructures

12 g of $Na_2SiO_3 \cdot 5H_2O$ were dissolved in about 50 mL of distilled water. 3 g of $MgCl_2 \cdot 6H_2O$ were dissolved in about 30 mL of distilled water. Using a pipette, the magnesium solution was added to the silicon solution drop by drop with continuous stirring for an hour. After that, the produced white gel was charged into a 100 mL Teflon-lined stainless-steel autoclave then the autoclave was placed inside a drying furnace at 150 °C for 12 h. Furthermore, the formed nanostructures were filtered, washed with hot distilled water, dried at 60 °C, and encoded as H1.

2.2.2. Synthesis of chitosan nanocomposite

125 mL of an acetic acid solution (5% V/V) was added to 2 g of chitosan and 2 g of the synthesized nanostructures then the mixture was stirred for 5 h. After that, the mixture is added partially wise to 250 mL of 0.65 M of NaOH with continuous stirring for 5 h. Furthermore, the formed nanocomposite was filtered, washed with hot distilled water, dried at 60 °C, and encoded as H1Ch.

2.3. Instrumentation

X-ray diffraction analyses of the H1 and H1Ch samples were carried out using a D8 Advance X-ray diffractometer (Billerica, Massachusetts, United States). Infrared analyses of the H1 and H1Ch samples were carried out using a Nicolet 6700 FT-IR spectrometer (Waltham, Massachusetts, United States). A JSM 6490 LV scanning electron microscope (Akishima, Tokyo, Japan) attached with an energy dispersive X-ray unit was employed to investigate the morphological structures and elemental compositions of the H1 and H1Ch samples. The concentrations of methylene blue and crystal violet dyes were determined using a Shimadzu 1800 UV–Vis spectrophotometer (Colmworth, United Kingdom). The maximum wavelengths of the methylene blue and crystal violet dyes are 663 and 590 nm, respectively. The percentages of carbon (C), hydrogen (H), and nitrogen (N) of the H1Ch nanocomposite

were determined using a 2400 PerkinElmer CHN Elemental analyzer (Waltham, United States).

2.4. Removal of methylene blue and crystal violet dye from aqueous media

0.1 g of the adsorbent (H1 or H1Ch) was added to 50 mL of 40 mg/L dye solution (methylene blue or crystal violet). The pH of the mixture was adjusted to the desired value using 0.1 M HCl or NaOH. The mixture was magnetically stirred at the desired time. The adsorbent was centrifuged then the concentration of methylene blue or crystal violet dyes was measured by a Shimadzu 1800 UV–Vis spectrophotometer. Several factors affecting the adsorption process have been studied such as pH (2–8), time (10–80 min), temperature (298–328 K), and concentration (20–60 mg/L). The % removal (% R) of the studied dyes and the adsorption capacity (Q) of
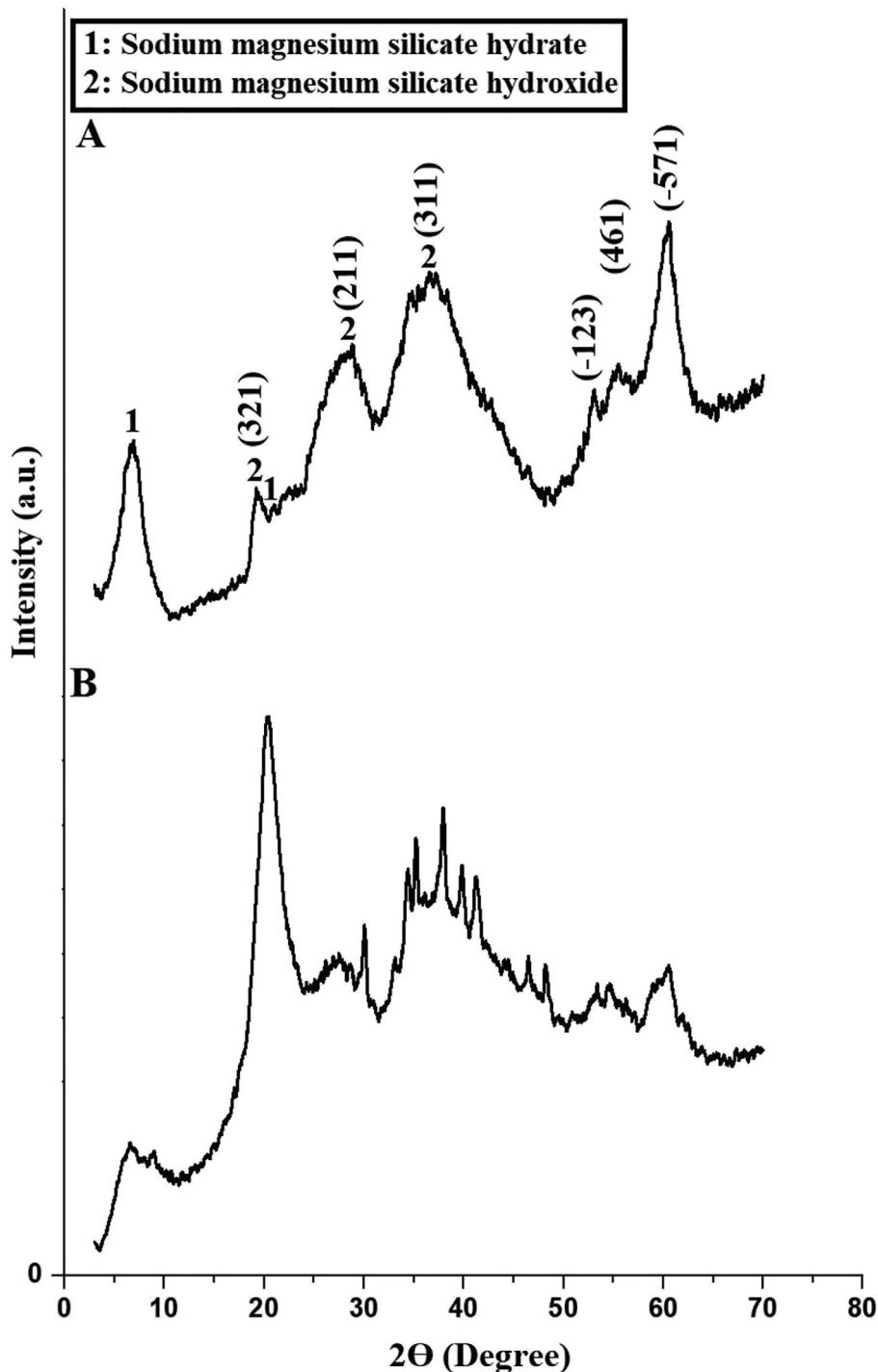

Fig. 1 The XRD patterns of the H1 (A) and H1Ch (B) samples.

the H1 or H1Ch adsorbents were determined using Eqs. (1) and (2), respectively.

$$\%R = \frac{C_o - C_e}{C_o} \times 100 \qquad (1)$$

$$Q = (C_o - C_e) \times \frac{V}{M} \qquad (2)$$

where, C_o is the initial concentration of the studied dyes (mg/L), C_e is the concentration of the studied dyes at equilibrium (mg/L), V is the volume of the dye solution (L), and M is the mass of the adsorbent (g).

3. Results and discussion

3.1. Characterization of the synthesized samples

3.1.1. X-ray diffraction

Fig. 1. **A-B** represents the XRD patterns of the H1 and H1Ch samples, respectively. The results confirmed that the H1 sample consists of two phases, namely sodium magnesium silicate hydroxide (Chemical formula: $Na(NaMg)Mg_5(Si_8O_{22}(OH)_2)$ and JCPDS No. 01–073-2764) and sodium magnesium silicate hydrate (Chemical formula: $Na_2Mg_3Si_6O_{16} \cdot 8H_2O$ and JCPDS No. 00–013-0310). The average crystallite size of the H1 sample is 90.27 nm. The observed peaks at $2\Theta = 6.71°$ and $20.80°$ are due to the sodium magnesium silicate hydrate. Also, the observed peaks at $2\Theta = 19.17°, 28.69°, 36.61°, 53.11°, 55.49°,$ and $60.47°$ are due to the (3 2 1), (2 1 1), (3 1 1), (−1 2 3), (4 6 1), and (−5 7 1) miller indices of the sodium magnesium silicate hydroxide, respectively. After the union of nanostructures with chitosan, as suggested in scheme 1, the characteristic peaks of chitosan at $2\Theta = 8.9°$ and $21°$ appeared very clearly, whereas the intensity of the other peaks was affected. These observations are consistent with other inorganic/organic nanocomposites prepared in similar ways as reported by Al-Wasidi et al. (Al-Wasidi et al., 2022a) (Al-Wasidi et al., 2022b) and Abdelrahman et al. (Abdelrahman and Hegazey, 2019a, 2019b).

3.1.2. EDX and CHN analyses

Fig. 2. **A-B** represents the EDX patterns of the H1 and H1Ch samples, respectively. The results confirmed that the H1 sample consists of Si, Mg, Na, and O with weight percentages equal to 41.5 0%, 16.33%, 5.59%, and 36.58%, respectively. Also, the H1Ch sample consists of Si, Mg, Na, O, C, and N with weight percentages equal to 7.24%, 5.73%, 10.59%, 30.99%, 43.25%, and 2.20%, respectively. The low percentage of silicon and the appearance of nitrogen and carbon in the H1Ch sample are the results of the association of chitosan with the synthesized nanostructures. Due to the functionalization of the nanostructures with chitosan, the CHN elemental analysis confirmed that the H1Ch sample contained C, H, and N with weight percentages equal to 53.28%, 4.32%, and 1.92%, respectively. These observations are consistent with other inorganic/organic nanocomposites prepared in similar ways as reported by Al-Wasidi et al. (Al-Wasidi et al., 2022a) (Al-Wasidi et al., 2022b) and Abdelrahman et al. (Abdelrahman and Hegazey, 2019a, 2019b).

3.1.3. FT-IR

Fig. 3. **A-B** represents the FT-IR spectra of the H1 and H1Ch samples, respectively. The results confirmed that the bands, which appeared at 454 and 662 cm^{-1} in the H1 and H1Ch samples, are due to the bending and internal symmetric stretching vibrations of L-O-L (L = Si and/or Mg), respectively. The bands, which appeared at 736 and 737 cm^{-1} in the H1 and H1Ch samples, are due to the external symmetric stretching of L-O-L, respectively. The bands, which appeared at 1011 and 1016 cm^{-1} in the H1 and H1Ch samples, are due to the internal asymmetric vibrations of L-O-L, respectively. The bands, which appeared at 1404 and 1417 cm^{-1} in the H1 and H1Ch samples, are due to the external asymmetric vibrations of L-O-L, respectively. The bands, which appeared at 1648 and 1573 cm^{-1} in the H1 and H1Ch samples, are due to the bending vibrations of O–H, respectively. The band, which appeared at 1653 cm^{-1} in the H1Ch sample, is due to bending vibration of NH$_2$. The bands, which appeared at 3471 and 3423 cm^{-1} in the H1 and H1Ch samples, are due to the stretch-
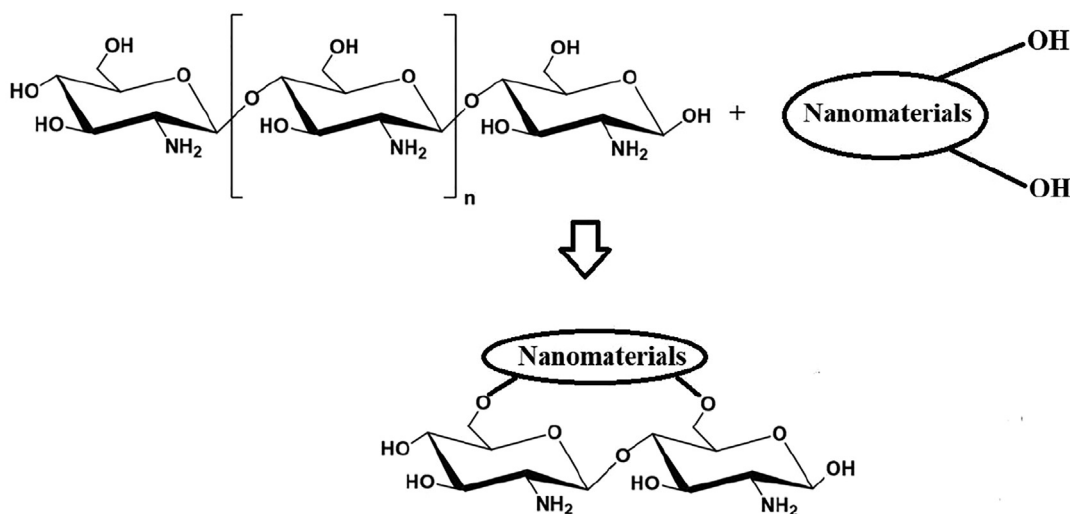
Scheme 1 Synthesis of chitosan nanocomposite.

ing vibrations of O–H and/or NH_2, respectively. The bands, which appeared at 1252 and 2914 cm^{-1} in the H1Ch sample, are due to the stretching vibrations of C-N and C–H, respectively. The bands, which appeared at 1063 and 1153 cm^{-1} in the H1Ch sample, are due to the stretching vibration of C-O (Abdelrahman and Hegazey, 2019a; Khalifa et al., 2020). These observations are consistent with other inorganic/organic nanocomposites prepared in similar ways as reported by Al-Wasidi et al. (Al-Wasidi et al., 2022a) (Al-Wasidi et al.,

2022b) and Abdelrahman et al. (Abdelrahman and Hegazey, 2019a, 2019b).

3.1.4. FE-SEM and surface area

Fig. 4. **A-B** represents the FE-SEM images of the H1 and H1Ch samples, respectively. The results confirmed that the H1 sample consists of spheres and irregular shapes. Also, the H1Ch sample consists of cotton and large irregular shapes due to the functionalization of the synthesized nanostructures
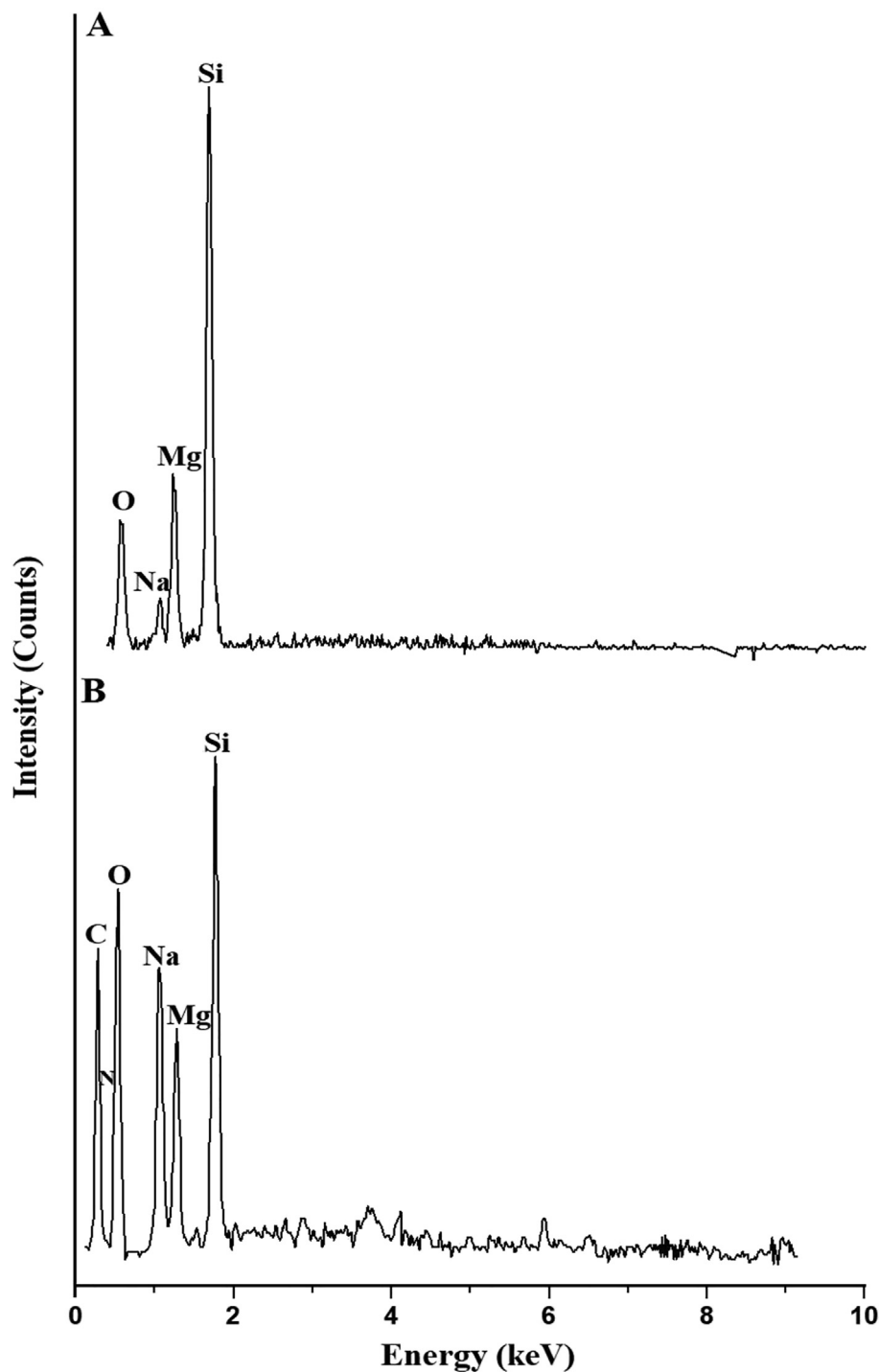

Fig. 2 The edx patterns of the h1 (a) and h1ch (b) samples.

with chitosan (Abdelrahman and Hegazey, 2019a; Khalifa et al., 2020). These observations are consistent with other inorganic/organic nanocomposites prepared in similar ways as reported by Al-Wasidi et al. (Al-Wasidi et al., 2022a) (Al-Wasidi et al., 2022b) and Abdelrahman et al. (Abdelrahman and Hegazey, 2019a, 2019b).

The BET surface area, which was determined using N_2 adsorption/desorption analyzer, of the H1 and H1Ch samples are 200.25 and 160.14 m^2/g, respectively. The decrease in the surface area of the H1Ch is due to the functionalization of the synthesized nanostructures with chitosan. Hence, the H1Ch can remove the cationic dyes (i.e., methylene blue and crystal violet dyes) via chemical electrostatic attraction between dyes and functional groups (i.e., NH_2 and OH) of the H1Ch adsorbent in basic medium. Also, the H1 sample can remove the cationic dyes via the ion exchange between sodium ions of the nanostructures and cationic dyes.

3.2. Removal of methylene blue and crystal violet dyes from aqueous media

3.2.1. Effect of pH

Fig. 5. A-B shows the plot of pH versus % R of the studied dyes and Q of the H1 and H1Ch samples, respectively. The results showed an increase in the values of % R and Q with an increase in pH from 2 to 8. Hence, pH = 8 is the ideal value at which other factors affecting the removal of the examined dyes will be studied. % R of methylene blue dye using the H1 and H1C samples at pH = 8 equals 71.25 and 93.75 %, respectively. Q of the H1 and H1C samples toward methylene blue dye equals 14.25 and 18.75 mg/g, respectively. % R of crystal violet dye using the H1 and H1C samples at pH = 8 equals 78.93 and 96.90 %, respectively. Q of the H1 and H1C samples toward crystal violet dye equals 15.79 and 19.38 mg/g, respectively.

3.2.2. Effect of time

Fig. 6. A-B shows the plot of time versus % R of the studied dyes and Q of the H1 and H1Ch samples, respectively. The results showed an increase in the values of % R and Q with an increase in time from 10 to 50 min. Also, there was approximate stability in both % R and Q when increasing the time from 50 to 80 min due to the saturation of active sites. Hence, time = 50 min is the ideal value at which other factors affecting the removal of the examined dyes will be studied. % R of methylene blue dye using the H1 and H1C samples after 50 min equals 72.50 and 93.88 %, respectively. Q of the H1 and H1C samples toward methylene blue dye equals 14.50 and 18.78 mg/g, respectively. % R of crystal violet dye using the H1 and H1C samples after 50 min equals 78.75 and
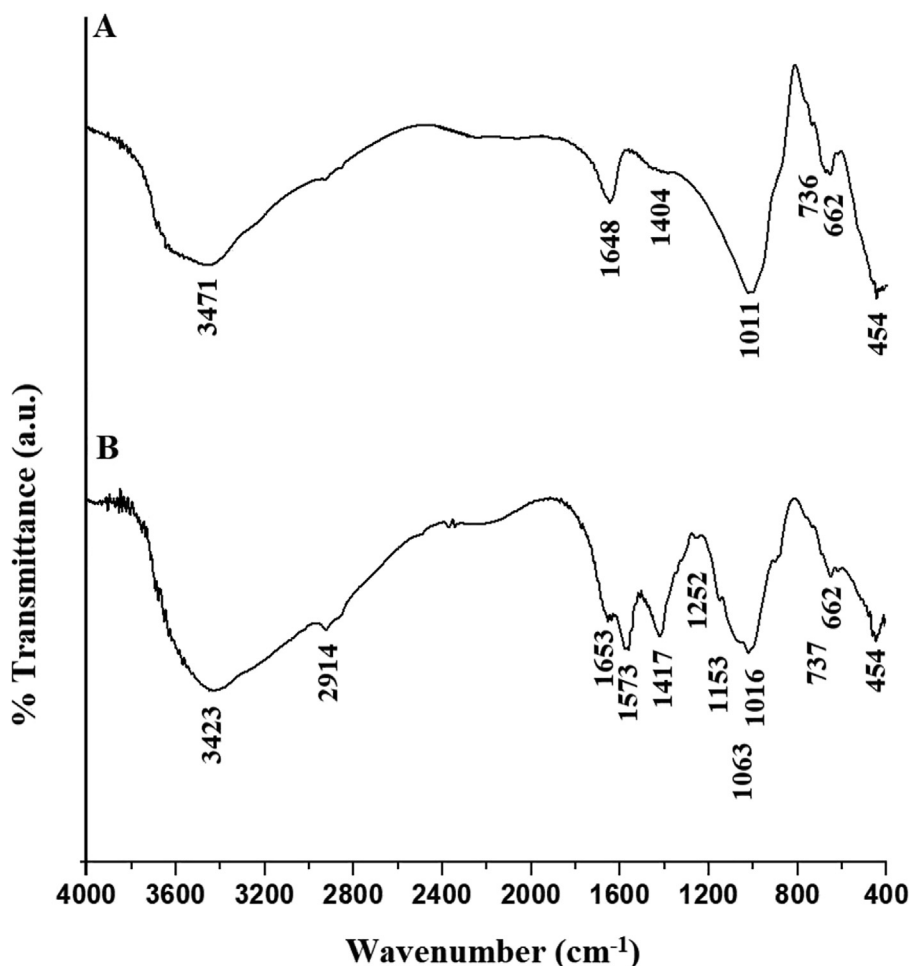

Fig. 3   The FT-IR spectra of the H1 (A) and H1Ch (B) samples.

97.00 %, respectively. Q of the H1 and H1C samples toward crystal violet dye equals 15.75 and 19.40 mg/g, respectively. The pseudo-first and pseudo-second-order kinetics, as expressed in Eqs. (3) and (4), were used to examine experimental data (Abdelrahman and Hegazey, 2019a; Khalifa et al., 2020).

$$\log (Q_e - Q_t) = logQ_e - \frac{k_1}{2.303}t \qquad (3)$$

$$\frac{t}{Q_t} = \frac{1}{k_2 Q_e^2} + \frac{1}{Q_e}t \qquad (4)$$

where, Q_e (mg/g) and Q_t (mg/g) are the quantities of adsorbed methylene blue or crystal violet dye per unit weight of the H1 or H1Ch samples at equilibrium and time t, respectively. Also, k_1 (1/min) and k_2 (g/mg.min) are the rate constant of the pseudo-first and pseudo-second-order models, respectively. Fig. 7. A-B shows the plot of time versus log (Q_e-Q_t) and t/Q_t, respectively. The values of k_1, k_2, Q_e, and correlation coefficients (R^2) are listed in Tables 1 and 2. The results are consistent with the pseudo-second-order because the R^2 values of the pseudo-second-order are more than R^2 values of the pseudo-first-order.
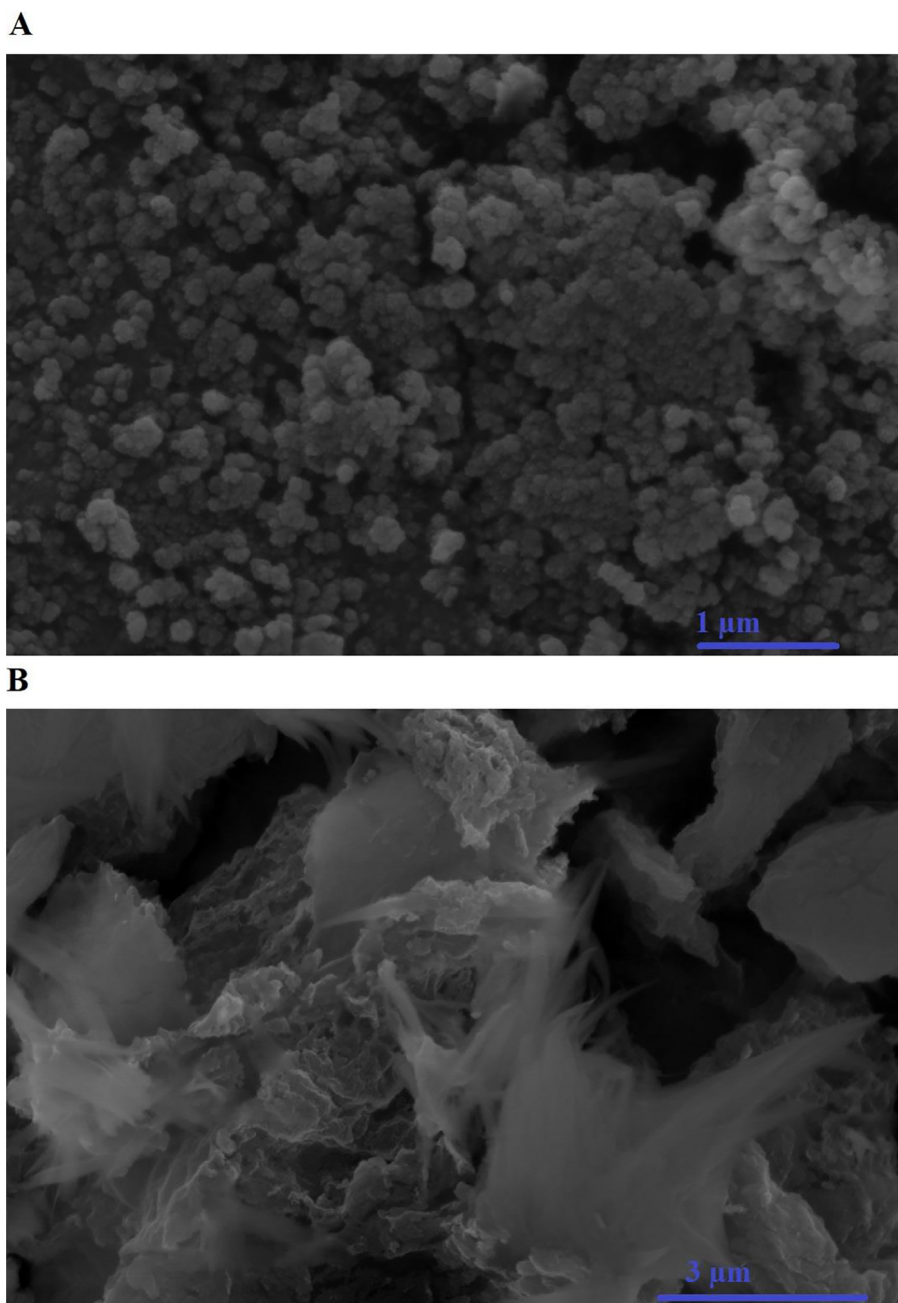
A

B

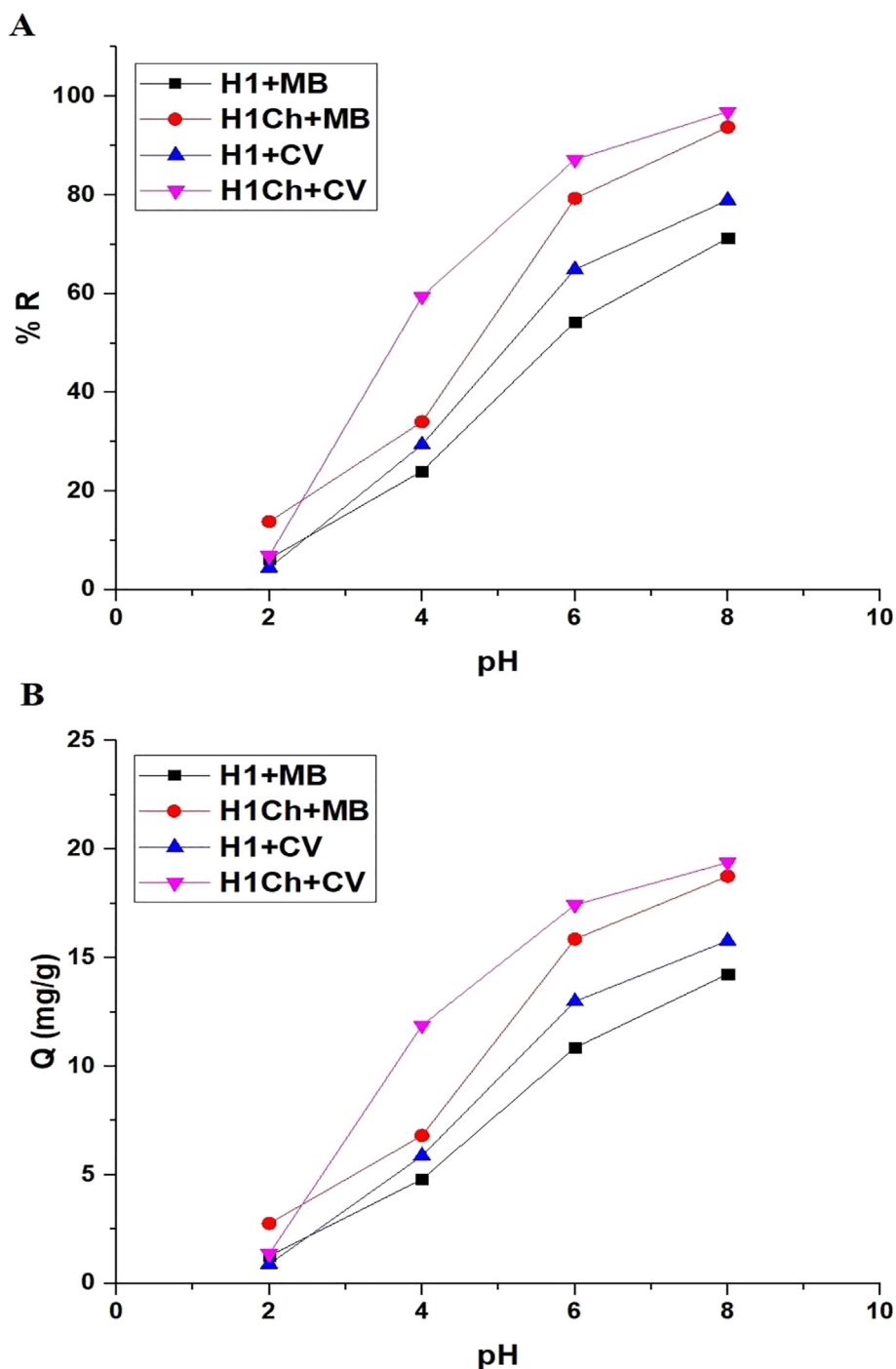Fig. 4 The FE-SEM images of the H1 and H1Ch samples, respectively.

Fig. 5 The plot of pH versus % R of the studied dyes (A) and Q of the H1 and H1Ch samples (B).

3.2.3. Effect of temperature

Fig. 8. A-B shows the plot of temperature versus % R of the studied dyes and Q of the H1 and H1Ch samples, respectively. The results showed a decrease in the values of % R and Q with an increase in temperature from 298 to 328 K. Hence, temperature = 298 K is the ideal value at which other factors affecting the removal of the examined dyes will be studied. The influence of temperature on the adsorption processes of the methylene blue and crystal violet dyes can be evaluated by

determining the thermodynamic parameters such as change in free energy ($\triangle G^o$, KJ/mol), change in entropy ($\triangle S^o$, KJ/-molK), and change in enthalpy ($\triangle H^o$, KJ/mol) applying Eqs. (5), (6), and (7) (Abdelrahman and Hegazey, 2019a; Khalifa et al., 2020).

$$lnK_d = \frac{\Delta S^o}{R} - \frac{\Delta H^o}{RT} \tag{5}$$

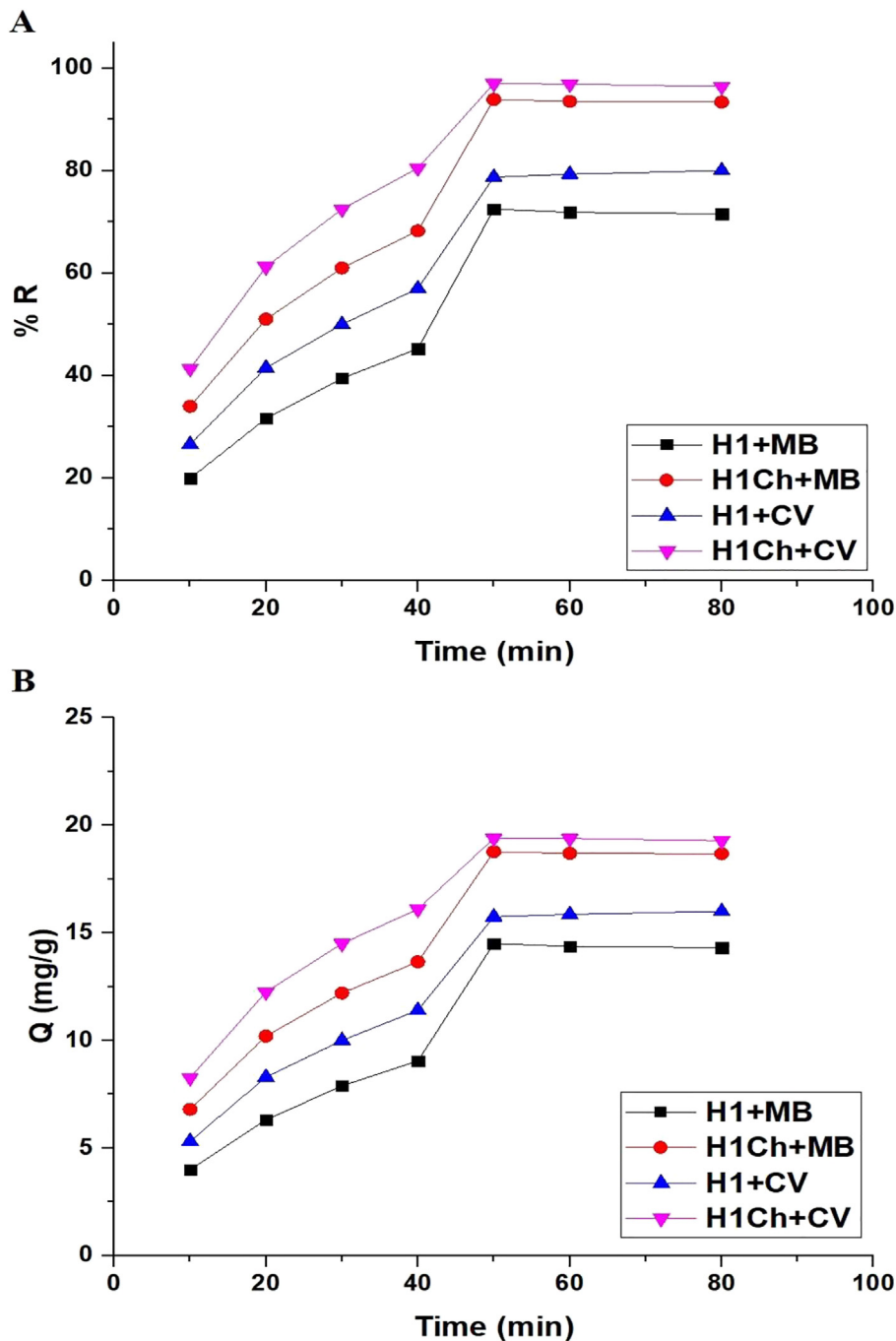$$\Delta G^o = \Delta H^o - T\Delta S^o \tag{6}$$

Fig. 6 The plot of time versus % R of studied dyes (A) and Q of the H1 and H1Ch samples (B).

$$K_d = \frac{Q_e}{C_e} \tag{7}$$

T (kelvin) is the adsorption temperature whereas K_d (L/g) is the distribution constant. R (kJ/mol kelvin) is a gas constant. By plotting ln K_d against 1/T, the $\triangle S^o$ and $\triangle H^o$ can be calculated from the intercept and slope as clarified in Fig. 9 and Tables 3 and 4. Additionally, the values of $\triangle G^o$ were calculated based on the values of $\triangle H^o$ and $\triangle S^o$, as clarified in Tables 3 and 4. The minus values of $\triangle H^o$ signifies that the adsorption processes are exothermic. In addition, $\triangle H^o$ is higher than 40 KJ/mol, which indicates the chemical adsorp-

tion. The positive values of ($\triangle S^o$) suggest greater randomization at the solid/solution interface after adsorption of the methylene blue and crystal violet dyes onto the H1 and H1Ch samples. The negative values of $\triangle G^o$ suggested the spontaneous nature of the adsorption of methylene blue and crystal violet dyes using the H1 and H1Ch samples.

3.2.4. Effect of concentration
Fig. 10. A-B shows the plot of concentration versus % R of the studied dyes and Q of the H1 and H1Ch samples, respectively. The results showed a decrease in the values of % R and an
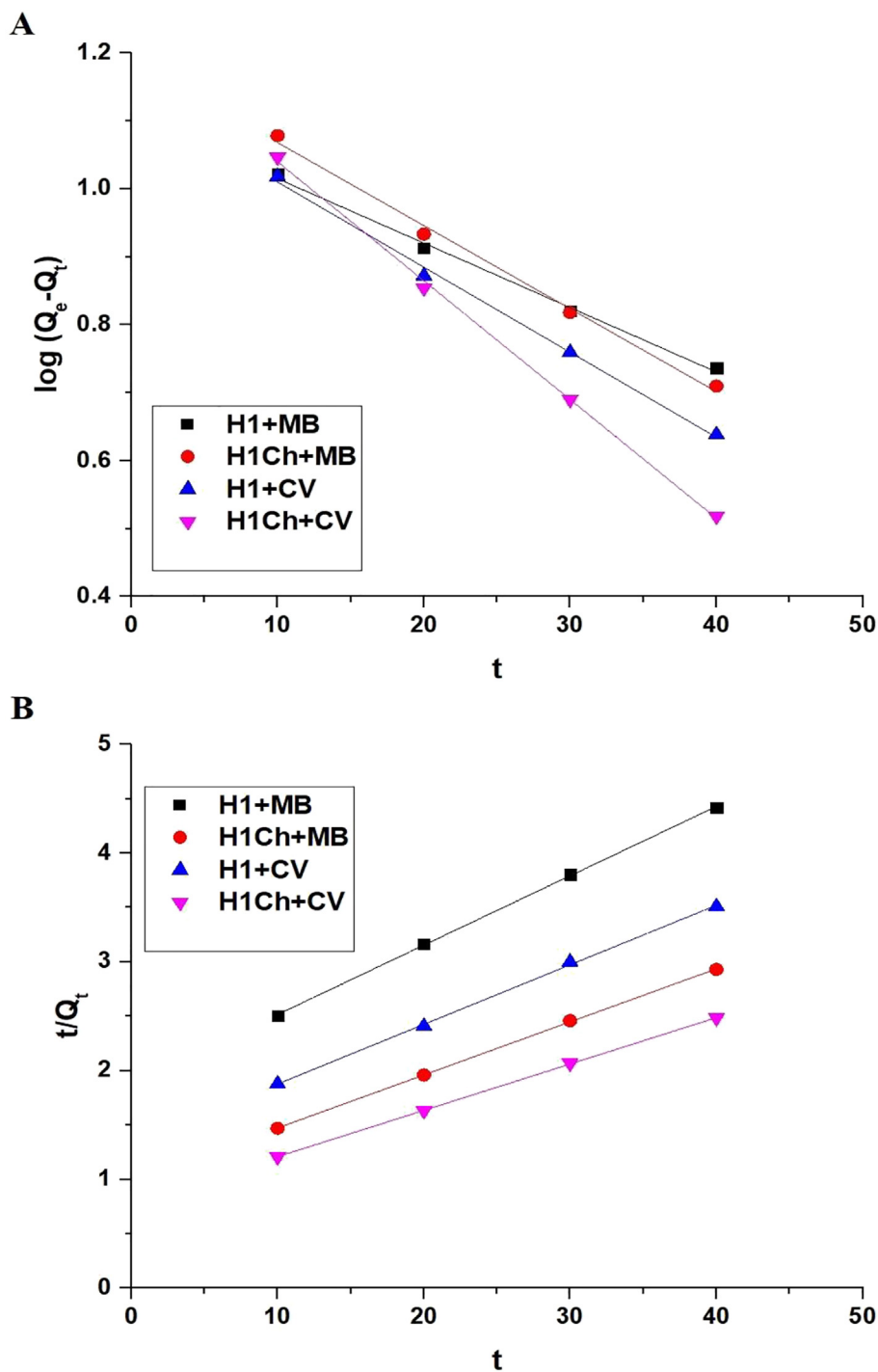
A

B

Fig. 7　The plot of time versus log (Q_e-Q_t) (A) and t/Q_t (B).

Table 1　The constants of the pseudo-first and pseudo-second-order models for the removal of methylene blue dye using the H1 and H1Ch samples.

Adsorbent	Pseudo-first-order			Pseudo-second-order		
	Q_e (mg/g)	k_1 (1/min)	R^2	Q_e (mg/g)	k_2 (g/mg.min)	R^2
H1	12.88	0.0218	0.9948	15.68	0.0022	0.9997
H1Ch	15.49	0.0281	0.9927	20.50	0.0024	0.9998

Table 2 The constants of the pseudo-first and pseudo-second-order models for the removal of crystal violet dye using the H1 and H1Ch samples.

Adsorbent	Pseudo-first-order			Pseudo-second-order		
	Q_e (mg/g)	k_1 (1/min)	R^2	Q_e (mg/g)	k_2 (g/mg.min)	R^2
H1	13.65	0.0288	0.9953	18.25	0.0023	0.9989
H1Ch	16.38	0.0403	0.9984	23.46	0.0024	0.9999
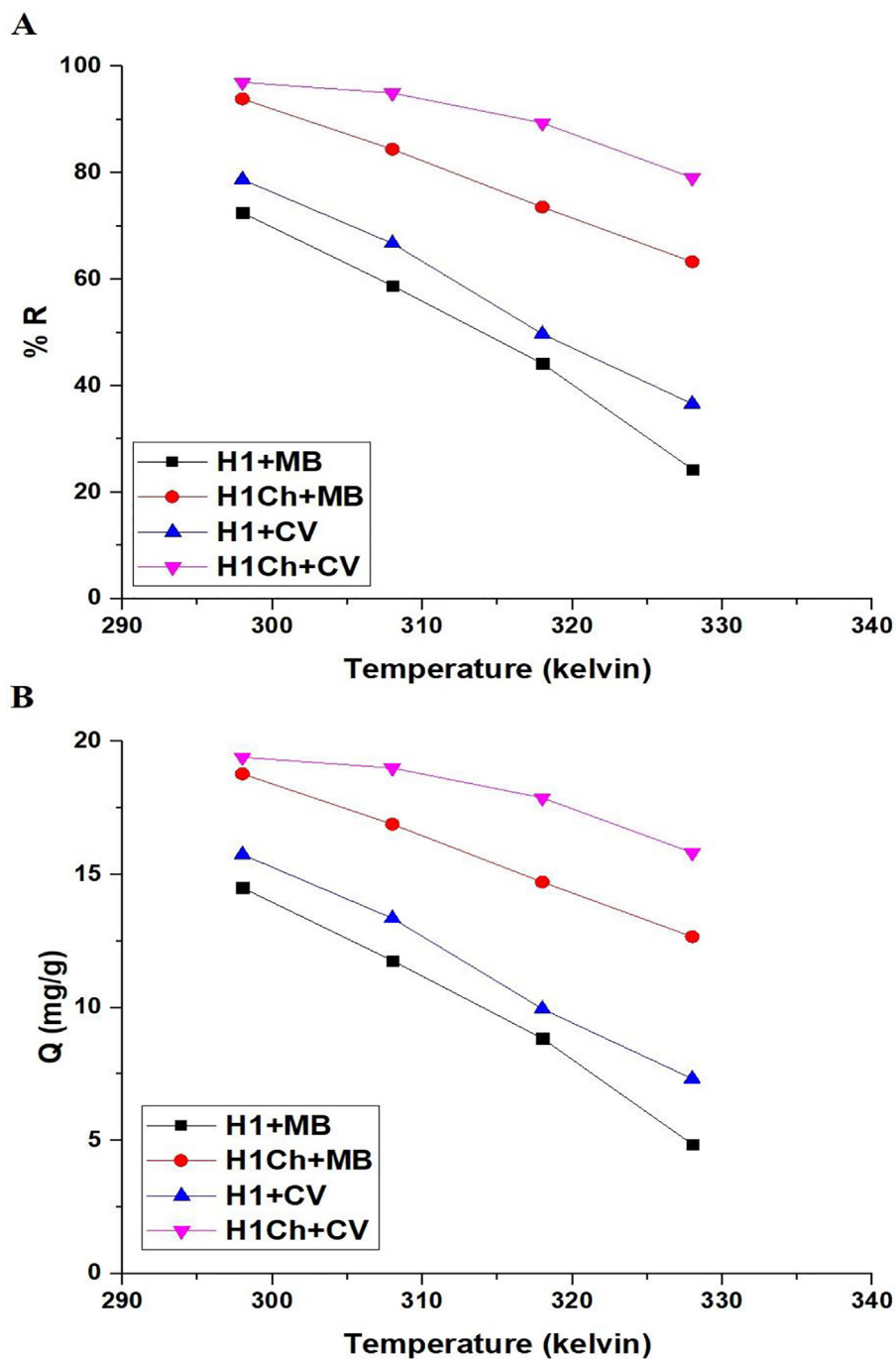
Fig. 8 The plot of temperature versus % R of the studied dyes (A) and Q of the H1 and H1Ch samples (B).
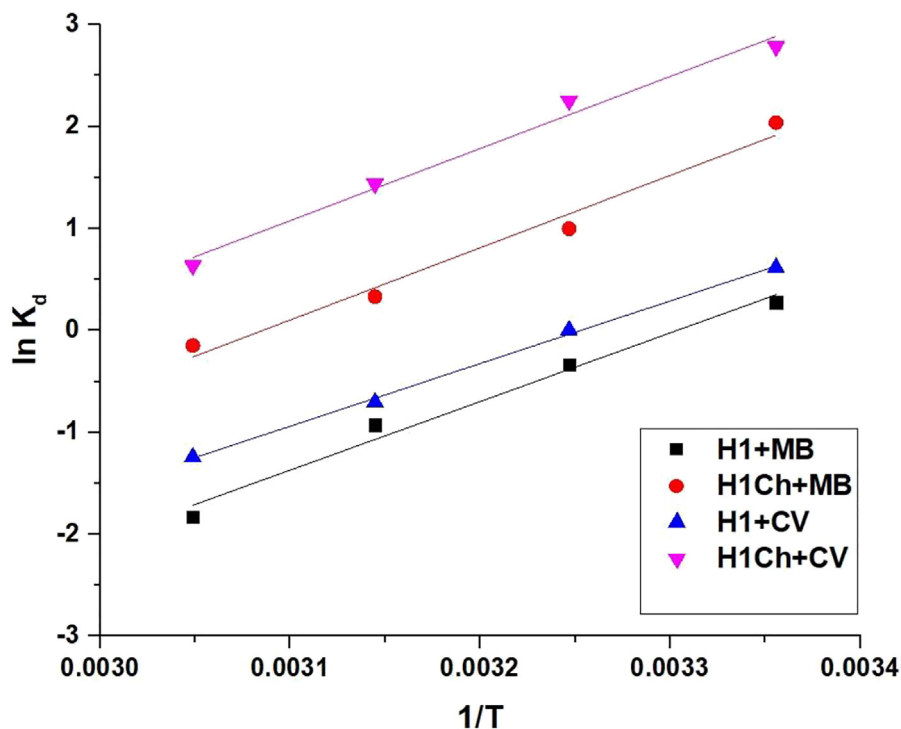
Fig. 9   The plot of 1/T versus ln K_d.

Table 3   The thermodynamic parameters for the removal of methylene blue dye using the H1 and H1Ch samples.

Adsorbent	$\triangle H^o$ (KJ/mol)	$\triangle S^o$ (KJ/mol kelvin)	$\triangle G^o$ (KJ/mol)			
			298	308	318	328
H1	−56.25	0.1858	−111.62	−113.48	−115.34	−117.19
H1Ch	−59.25	0.1828	−113.73	−115.56	−117.39	−119.22

Table 4   The thermodynamic parameters for the removal of crystal violet dye using the H1 and H1Ch samples.

Adsorbent	$\triangle H^o$ (KJ/mol)	$\triangle S^o$ (KJ/mol kelvin)	$\triangle G^o$ (KJ/mol)			
			298	308	318	328
H1	−51.34	0.1669	−101.09	−102.77	−104.44	−106.11
H1Ch	−59.10	0.1742	−111.02	−112.76	−114.50	−116.25

increase in the values of Q with an increase in concentration from 20 to 60 mg/L. The Langmuir and Freundlich isotherms, as expressed in Eqs. (8) and (9), were used to examine experimental data (Abdelrahman and Hegazey, 2019a; Khalifa et al., 2020).

$$\frac{C_e}{Q_e} = \frac{1}{k_L Q_m} + \frac{C_e}{Q_m} \qquad (8)$$

$$lnQ_e = lnk_F + \frac{1}{n}lnC_e \qquad (9)$$

k_L (L/mg) is the equilibrium constant of the Langmuir isotherm whereas Q_m (mg/g) is the maximum adsorption capacity of the Langmuir isotherm. k_F (mg/g)(L/mg)$^{1/n}$ and 1/n are the equilibrium constant and the heterogeneity constant of the Freundlich isotherm, respectively. The Freundlich isotherm can be utilized to determine the Q_m using Eq. (10) (Abdelrahman and Hegazey, 2019a; Khalifa et al., 2020).

$$Q_m = k_F\left(C_o^{\frac{1}{n}}\right) \qquad (10)$$

Fig. 11. A-B shows the Langmuir and Freundlich isotherms, respectively. The values of k_L, k_F, Q_m, and correlation coefficients (R^2) are listed in Tables 5 and 6. The results are consistent with the Langmuir isotherm because the R^2 values of the Langmuir isotherm are more than the R^2 values of the Freundlich isotherm. The maximum adsorption capacity of the H1 and H1Ch samples toward

the methylene blue dye is 19.07 and 20.25 mg/g, respectively. Also, the maximum adsorption capacity of the H1 and H1Ch samples toward the crystal violet dye is 18.62 and 23.51 mg/g, respectively. Nonlinear equilibrium isotherms were studied as described by Altowayti et al. (Figures omitted for brevity). The R^2 value derived from the nonlinear plot is much smaller than that derived from the linear isotherm. Hence, the results of this study showed that the linear method is a good way to show the equilibrium data (Altowayti et al., 2021).
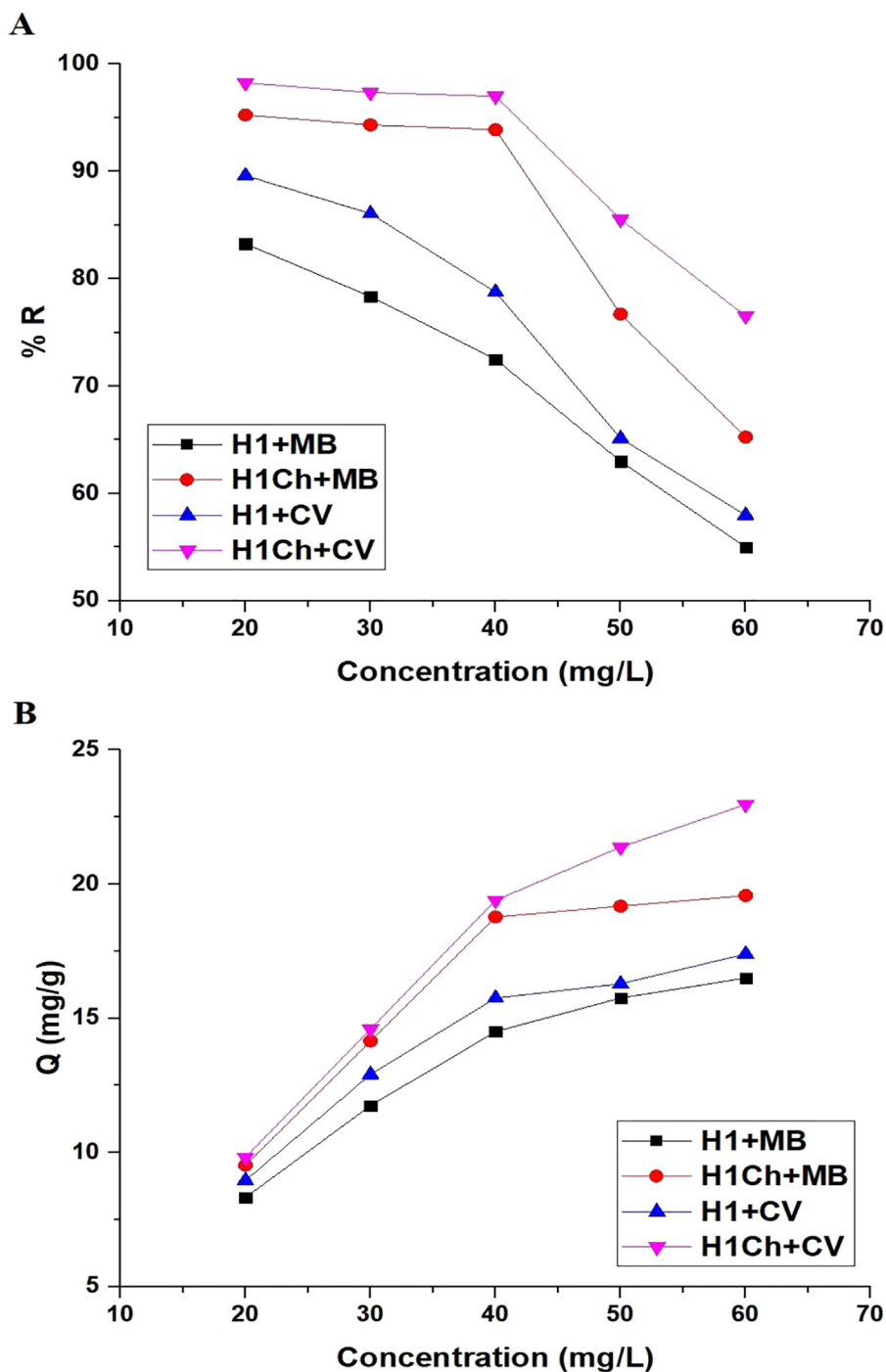

Fig. 10 The plot of concentration versus % R of the studied dyes (A) and Q of the H1 and H1Ch samples (B).
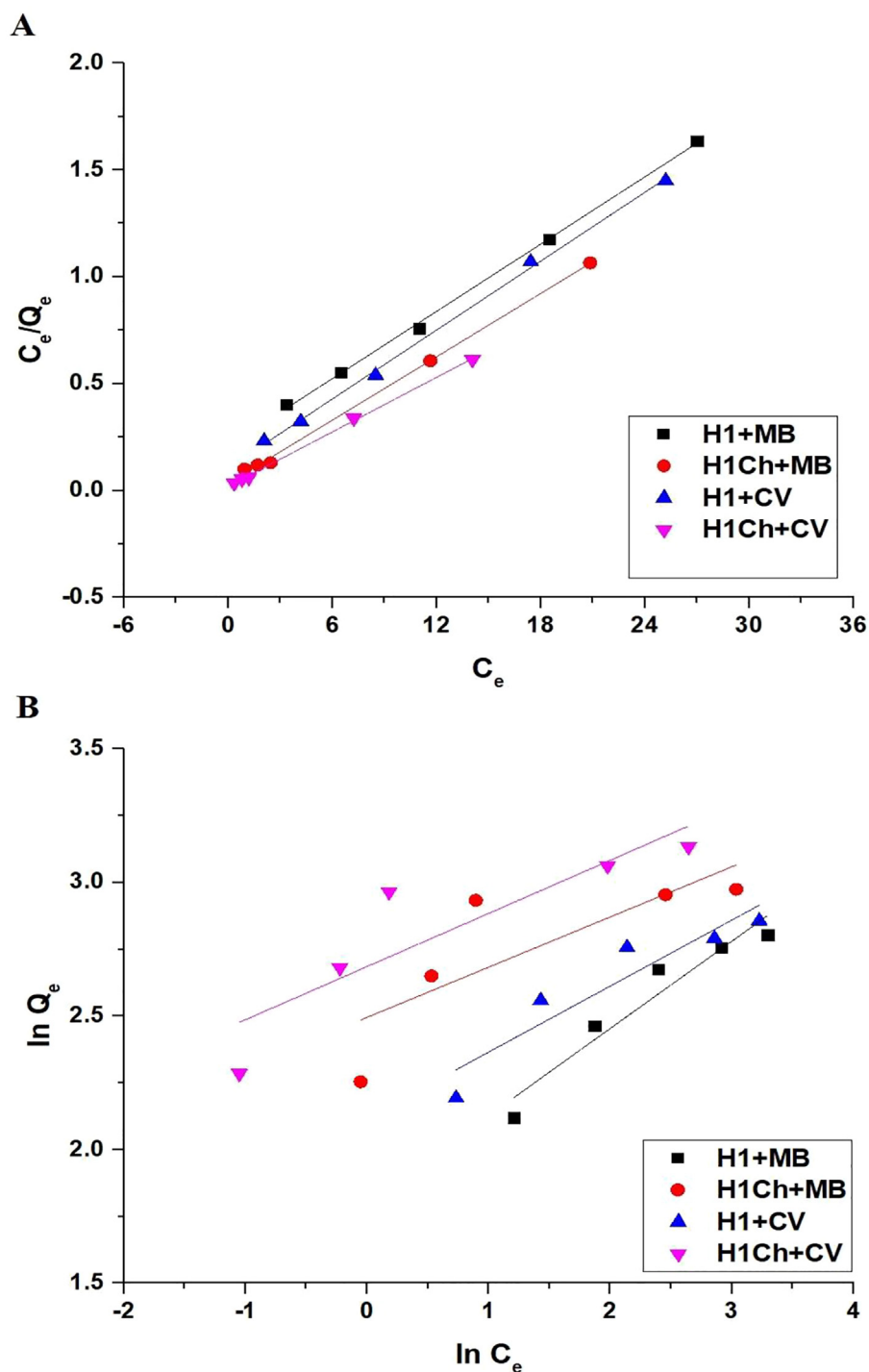
Fig. 11 The Langmuir (A) and Freundlich (B) isotherms.

Table 5 The constants of the Langmuir and Freundlich isotherms for the removal of methylene blue dye using the H1 and H1Ch samples.

Adsorbent	Langmuir			Freundlich		
	Q_m (mg/g)	k_L (L/mg)	R^2	Q_m (mg/g)	k_F (mg/g)(L/mg)$^{1/n}$	R^2
H1	19.07	0.2505	0.9984	20.16	6.0555	0.9063
H1Ch	20.25	1.4856	0.9982	24.23	12.1187	0.5194

Table 6 The constants of the Langmuir and Freundlich isotherms for the removal of crystal violet dye using the H1 and H1Ch samples.

Adsorbent	Langmuir			Freundlich		
	Q_m (mg/g)	k_L (L/mg)	R^2	Q_m (mg/g)	k_F (mg/g)(L/mg)$^{1/n}$	R^2
H1	18.62	0.5047	0.9979	20.67	8.3138	0.8362
H1Ch	23.51	2.1869	0.9988	30.53	14.66	0.7134

4. Conclusions

The hydrothermal method was utilized for the facile synthesis of sodium magnesium silicate hydroxide/sodium magnesium silicate hydrate nanostructures. The nanostructures were modified by chitosan as a novel composite for the efficient removal of the methylene blue and crystal violet dyes from aqueous media. The functionalization of nanostructures with chitosan led to the appearance of chitosan XRD peaks at $2\Theta = 8.9°$ and $21°$ whereas the intensities of the other XRD peaks were affected. The maximum adsorption capacity of the nanostructures and nanocomposite toward the methylene blue dye is 19.07 and 20.25 mg/g, respectively. Also, the maximum adsorption capacity of the nanostructures and nanocomposite toward the crystal violet dye is 18.62 and 23.51 mg/g, respectively.

Declaration of Competing Interest

The authors declare that they have no known competing financial interests or personal relationships that could have appeared to influence the work reported in this paper.

References

Abdelrahman, E.A., 2018. Synthesis of zeolite nanostructures from waste aluminum cans for efficient removal of malachite green dye from aqueous media. J. Mol. Liq. 253, 72–82. https://doi.org/10.1016/j.molliq.2018.01.038.

Abdelrahman, E.A., Hegazey, R.M., 2019a. Utilization of waste aluminum cans in the fabrication of hydroxysodalite nanoparticles and their chitosan biopolymer composites for the removal of Ni(II) and Pb(II) ions from aqueous solutions: kinetic, equilibrium, and reusability studies. Microchem. J. 145, 18–25. https://doi.org/10.1016/j.microc.2018.10.016.

Abdelrahman, E.A., Hegazey, R.M., 2019b. Exploitation of Egyptian insecticide cans in the fabrication of Si/Fe nanostructures and their chitosan polymer composites for the removal of Ni(II), Cu(II), and Zn(II) ions from aqueous solutions. Compos. Part B Eng. 166, 382–400. https://doi.org/10.1016/j.compositesb.2019.02.027.

Abdelrahman, E.A., Hegazey, R.M., El-Azabawy, R.E., 2019a. Efficient removal of methylene blue dye from aqueous media using Fe/Si, Cr/Si, Ni/Si, and Zn/Si amorphous novel adsorbents. J. Mater. Res. Technol. 8, 5301–5313. https://doi.org/10.1016/j.jmrt.2019.08.051.

Abdelrahman, E.A., Hegazey, R.M., Kotp, Y.H., Alharbi, A., 2019b. Facile synthesis of Fe2O3 nanoparticles from Egyptian insecticide cans for efficient photocatalytic degradation of methylene blue and crystal violet dyes. Spectrochim. Acta - Part A Mol. Biomol. Spectrosc. 222,. https://doi.org/10.1016/j.saa.2019.117195 117195.

Adel, M., Ahmed, M.A., Mohamed, A.A., 2021. A facile and rapid removal of cationic dyes using hierarchically porous reduced graphene oxide decorated with manganese ferrite. FlatChem 26,. https://doi.org/10.1016/j.flatc.2021.100233 100233.

Altowayti, W.A.H., Othman, N., Goh, P.S., Alshalif, A.F., Al-Gheethi, A.A., Algaifi, H.A., 2021. Application of a novel nanocomposites carbon nanotubes functionalized with mesoporous

silica-nitrenium ions (CNT-MS-N) in nitrate removal: optimizations and nonlinear and linear regression analysis. Environ. Technol. Innov. 22,. https://doi.org/10.1016/j.eti.2021.101428 101428.

Al-Wasidi, A.S., AlSalem, H.S., Alshalawi, A.F., Naglah, A.M., Al-Anwar, A., Abdelrahman, E.A., 2022a. Facile synthesis of a novel nanocomposite for determination of mercury and copper ions in food and water samples. Arab. J. Chem. 15,. https://doi.org/10.1016/j.arabjc.2022.104113 104113.

Al-Wasidi, A.S., Naglah, A.M., Saad, F.A., Abdelrahman, E.A., 2022b. Modification of sodium aluminum silicate hydrate by thioglycolic acid as a new composite capable of removing and preconcentrating Pb(II), Cu(II), and Zn(II) ions from food and water samples. Arab. J. Chem. 15,. https://doi.org/10.1016/j.arabjc.2022.104178 104178.

Arif Ullah, M., Sulaiman Othman Alhar, M., Ullah Khan, A., Tahir, K., E. A. Zaki, M., Alabbad, E.A., Abdu Musad Saleh, E., M. A. Hassan, H., El-Zahhar, A.A., Munshi, A.M., 2023. Photocatalytic removal of alizarin red and photoinhibition of microbes in the presence of surfactant and Bio-template mediated Ag/SnO2/Nb2O5-SiO2 nanocomposite. J. Mol. Liq. 370, 121042. https://doi.org/10.1016/j.molliq.2022.121042

El-Aassar, M.R., Alezbaway, A.K., Althobaiti, I.O., El-Sayed, M.Y., Abu Salem, H.S., Hassan, H.M.A., Alolaimi, R.F., El Agammy, E.F., Mohy-Eldin, M.S., Mohamed, F.M., 2022. Fabrication of novel Bentonite-Anthracite@Zetag (BT-An@Zetag) composite for the removal of Arsenic (V) from an aqueous solution. Molecules 27. https://doi.org/10.3390/molecules27217635.

Elgarahy, A.M., Elwakeel, K.Z., Mohammad, S.H., Elshoubaky, G.A., 2021. A critical review of biosorption of dyes, heavy metals and metalloids from wastewater as an efficient and green process. Clean. Eng. Technol. 4,. https://doi.org/10.1016/j.clet.2021.100209 100209.

Fetimi, A., Dâas, A., Benguerba, Y., Merouani, S., Hamachi, M., Kebiche-Senhadji, O., Hamdaoui, O., 2021. Optimization and prediction of safranin-O cationic dye removal from aqueous solution by emulsion liquid membrane (ELM) using artificial neural network-particle swarm optimization (ANN-PSO) hybrid model and response surface methodology (RSM). J. Environ. Chem. Eng. 9. https://doi.org/10.1016/j.jece.2021.105837.

Hotan Alsohaimi, I., Alhumaimess, M.S., Abdullah Alqadami, A., Tharwi Alshammari, G., Fawzy Al-Olaimi, R., Abdeltawab, A.A., El-Sayed, M.Y., Hassan, H.M., 2023. Adsorptive performance of aminonaphthalenesulfonic acid modified magnetic-graphene oxide for methylene blue dye: mechanism, isotherm and thermodynamic studies. Inorg. Chem. Commun. 147,. https://doi.org/10.1016/j.inoche.2022.110261 110261.

Karaman, C., Karaman, O., Show, P.L., Karimi-Maleh, H., Zare, N., 2022. Congo red dye removal from aqueous environment by cationic surfactant modified-biomass derived carbon: equilibrium, kinetic, and thermodynamic modeling, and forecasting via artificial neural network approach. Chemosphere 290,. https://doi.org/10.1016/j.chemosphere.2021.133346 133346.

Karimi-Maleh, H., Darabi, R., Karimi, F., Karaman, C., Shahidi, S.A., Zare, N., Baghayeri, M., Fu, L., Rostamnia, S., Rouhi, J., Rajendran, S., 2023. State-of-art advances on removal, degradation and electrochemical monitoring of 4-aminophenol pollutants in

real samples: a review. Environ. Res. 222,. https://doi.org/10.1016/j.envres.2023.115338 115338.

Khalifa, M.E., Abdelrahman, E.A., Hassanien, M.M., Ibrahim, W.A., 2020. Application of mesoporous silica nanoparticles modified with Dibenzoylmethane as a novel composite for efficient removal of Cd (II), Hg(II), and Cu(II) ions from aqueous media. J. Inorg. Organomet. Polym. Mater. 30, 2182–2196. https://doi.org/10.1007/s10904-019-01384-w.

Konicki, W., Cendrowski, K., Bazarko, G., Mijowska, E., 2015. Study on efficient removal of anionic, cationic and nonionic dyes from aqueous solutions by means of mesoporous carbon nanospheres with empty cavity. Chem. Eng. Res. Des. 94, 242–253. https://doi.org/10.1016/j.cherd.2014.08.006.

Liu, C., Omer, A.M., Ouyang, X. kun, 2018. Adsorptive removal of cationic methylene blue dye using carboxymethyl cellulose/k-carrageenan/activated montmorillonite composite beads: Isotherm and kinetic studies. Int. J. Biol. Macromol. 106, 823–833. https://doi.org/10.1016/j.ijbiomac.2017.08.084

Luo, X., Zhang, L., 2009. High effective adsorption of organic dyes on magnetic cellulose beads entrapping activated carbon. J. Hazard. Mater. 171, 340–347. https://doi.org/10.1016/j.jhazmat.2009.06.009.

Mahmoud, M.E., Nabil, G.M., Khalifa, M.A., El-Mallah, N.M., Hassouba, H.M., 2019. Effective removal of crystal violet and methylene blue dyes from water by surface functionalized zirconium silicate nanocomposite. J. Environ. Chem. Eng. 7,. https://doi.org/10.1016/j.jece.2019.103009 103009.

Marsiezade, N., Javanbakht, V., 2020. Novel hollow beads of carboxymethyl cellulose/ZSM-5/ZIF-8 for dye removal from aqueous solution in batch and continuous fixed bed systems. Int. J. Biol. Macromol. 162, 1140–1152. https://doi.org/10.1016/j.ijbiomac.2020.06.229.

Oladoye, P.O., Ajiboye, T.O., Omotola, E.O., Oyewola, O.J., 2022. Methylene blue dye: toxicity and potential elimination technology from wastewater. Results Eng. 16,. https://doi.org/10.1016/j.rineng.2022.100678 100678.

Priya, R., Nithya, R., Anuradha, R., Kamachi, T., 2014. Removal of colour from crystal violet dye using low cost adsorbents. Int. J. ChemTech Res. 6, 4346–4351.

Qiu, J., Feng, Y., Zhang, X., Jia, M., Yao, J., 2017. Acid-promoted synthesis of UiO-66 for highly selective adsorption of anionic dyes: adsorption performance and mechanisms. J. Colloid Interface Sci. 499, 151–158. https://doi.org/10.1016/j.jcis.2017.03.101.

Salisu, A., Sanagi, M.M., Karim, K.J.A., Pourmand, N., Ibrahim, W.A.W., 2015a. Adsorption of methylene blue on alginate-grafted-poly (methyl methacrylate). J. Teknol. 76, 19–25. https://doi.org/10.11113/jt.v76.5818.

Salisu, A., Sanagi, M.M., Naim, A.A., Karim, K.J., 2015b. Removal of methylene blue dye from aqueous solution using alginate grafted polyacrylonitrile beads. Der Pharma Chem. 7, 237–242.

Sankar Sana, S., Haldhar, R., Parameswaranpillai, J., Chavali, M., Kim, S.C., 2022. Silver nanoparticles-based composite for dye removal: a comprehensive review. Clean. Mater. 6,. https://doi.org/10.1016/j.clema.2022.100161 100161.

Shirani, M., Semnani, A., Haddadi, H., Habibollahi, S., 2014. Optimization of simultaneous removal of methylene blue, crystal violet, and fuchsine from aqueous solutions by magnetic NaY zeolite composite. Water. Air. Soil Pollut. 225. https://doi.org/10.1007/s11270-014-2054-2.

Wang, M., Fang, D., Yin, Q., Yi, J., Zeng, T., Ruzimuradov, O., Wang, M., Peng, S., Yao, D., 2022. Adsorption properties of methylene blue and gentian violet of sodium vanadate nanowire arrays synthesized by hydrothermal method. Appl. Surf. Sci. 604,. https://doi.org/10.1016/j.apsusc.2022.154608 154608.

Wasim, M., Sabir, A., Shafiq, M., Khan, R.U., 2022. Mussel inspired surface functionalization of polyamide membranes for the removal and adsorption of crystal violet dye. Dye. Pigment. 206,. https://doi.org/10.1016/j.dyepig.2022.110606 110606.